LAWRENCE
LIVERMORE
NATIONAL
LABORATORY

LLNL-JRNL-689346

Observation of Shock Compression-Induced BCC to HCP Phase Transformation in Tantalum Subjected to High Amplitude Pulser Laser

B. Remington, C. H. Lu, B. R. Maddox, H. S. Park

April 18, 2016

Scientific Reports

Disclaimer

This document was prepared as an account of work sponsored by an agency of the United States government. Neither the United States government nor Lawrence Livermore National Security, LLC, nor any of their employees makes any warranty, expressed or implied, or assumes any legal liability or responsibility for the accuracy, completeness, or usefulness of any information, apparatus, product, or process disclosed, or represents that its use would not infringe privately owned rights. Reference herein to any specific commercial product, process, or service by trade name, trademark, manufacturer, or otherwise does not necessarily constitute or imply its endorsement, recommendation, or favoring by the United States government or Lawrence Livermore National Security, LLC. The views and opinions of authors expressed herein do not necessarily state or reflect those of the United States government or Lawrence Livermore National Security, LLC, and shall not be used for advertising or product endorsement purposes.

LLNL-JRNL-689346

Observation of Shock Compression-Induced BCC to HCP Phase Transformation in Tantalum Subjected to High Amplitude Pulsed Laser

C.-H. Lu[1], B. A. Remington[2], B. R. Maddox[2], H.-S. Park[2], M. A. Meyers[1]

[1]University of California, San Diego, La Jolla, CA, 92093, USA
[2] Lawrence Livermore National Laboratory, Livermore, CA, 94550, USA

Abstract

The formation of an hcp (Omega) phase was observed in recovered monocrystalline tantalum with orientations [001], [110], [111], and [123] subjected to laser driven shock compression at an energy around 650 J, generating a shock amplitude of about 70 GPa and duration of ~ 3.7 ns with an associated temperature of ~900 K. The substructures generated by the laser pulse were mainly characterized by transmission +electron microscopy. A VISAR experiment was used to predict the pressure decay profile in the metal and the corresponding value in the observation plane. It is proposed that the shear stresses generated in by the uniaxial strain state of shock compression play an important role in the transformation.

1. Introduction

Phase transitions are of utmost importance in the properties of materials. For instance, a displacive phase transformation (martensite) is responsible for the extraordinary range of strengths and toughness of steel, making it the most versatile and important structural material. The discovery of new phase transitions is not currently a common event and often requires a mix of experimentation, predictive computations, and luck. High energy pulsed lasers are enabling an expanding pressure and temperature regime and the exploration of extreme conditions.

Tantalum is an important metal and is being used globally as a model for the body centered cubic structure, receiving considerable attention. There is an ongoing experimental controversy on a possible high-pressure, high-temperature polymorphism in tantalum. Burakovsky et al. [1] conducted *ab initio* calculations (quantum molecular dynamics (QMD) simulations) that predicted the existence of an Omega (hcp) phase in the high pressure-temperature regime of monocrystalline Ta (above ~70 GPa). Using a density functional theory (DFT)-based model and generalized pseudopotential theory (MGPT) multi-ion interatomic potentials, Haskins et al. [2] found a size effect for the hexagonal phase. Shang et al. [3] systematically calculated phase transition pressures for 76 elemental solids including pure tantalum, mentioning a bcc-hcp transition at 67.5/285 GPa by using the projector-augmented wave method within the generalized gradient approximation.

Experimentally, Hsiung and Lassila [4–6] observed twins and Omega phase formed in pure Ta and Ta-W alloy. The bcc-to-hcp phase transition occurred in Ta-10W alloy at about 30 GPa and in polycrystalline Ta at 45 GPa with a 1.8 μs duration. They proposed a mechanism, indicating that shock pressure leads to shear-based transformation in tantalum from the bcc to the Omega phase. In sound velocity measurements of tantalum under shock compression, Hu et al. [7] mentioned that the kink at ~60 GPa in the observed longitudinal sound velocity may have been caused by a shock-induced phase transformation. Thus, the possible existence of the Omega phase has been discussed extensively in the literature and there is a considerable degree of uncertainty.

The objective of this report is to describe observations of a solid-solid phase transformation in monocrystalline tantalum with different orientations ([001], [110], [111], and

[123]) shock compressed at very short durations (~ 3ns) and high strain rate (~10^8/s) in a uniaxial strain state.

2. Experimental Techniques

Pure monocrystalline Ta with four orientations, [001], [110], [111], and [123], was obtained from MarkeTech Intl, Inc. in cylindrical shape with dimensions of 3 mm diameter and 3 mm height. The interstitial impurities (ppm in weight) measured by Evan Analytical Group (EAG) in Ta are O:<10, N:<10, H:7.6 and C:<10. The laser recovery experiments were performed at the Laboratory for Laser Energetics, University of Rochester (Omega Facility). The experimental set-up had previously been tested for recovery of FCC metals [8–13] and is described in detail elsewhere [14]. The cylindrical tantalum monocrystal targets were placed behind a tantalum washer inside a stainless steel recovery container. The samples were backed up by a Ta momentum trap to minimize reflected tensile pulses. The inside of this container was filled with silica aerogel, which acted as a deceleration medium for the tantalum specimens after they had undergone compression loading (Figure 1(a)).

VISAR (velocity interferometer system for any reflector) experiments of the drive were performed. The VISAR experiments were conducted on Al-LiF drive calibration samples and provided interface velocity data that allowed pressure versus time of the loading to be deduced, which became the input to the subsequent computer simulations. Based on the VISAR experiment and 1-D LASNEX simulations, the pressure decay profile in this experiment with different energy inputs can be established with considerable certainty. For a nominal input energy of 600 J, the predicted decay is shown in Fig. 1(b).

The shocked targets were examined using a scanning electron microscope (Phillips XL30 ESEM) and transmission electron microscope (Tecnai F20, operated at 200 kV). Transmission electron microscopy (TEM) foils were mainly prepared by focused ion beam (FIB; Hitachi NB-5000 FIB-SEM) techniques due to difficulties in electropolishing in the following three orientations: [110], [111], and [123]. The samples prepared for FIB were cut into half and mounted into epoxy. The cross-sections were mechanically polished using Al_2O_3 paste down to 0.05 µm and coated with a thin layer of Ir for the FIB milling procedure. The FIB samples were perpendicular to the shock propagation direction (and parallel to the surface of the Ta specimens) and had a thickness of 50-100 nm. There are two benefits from this cutting procedure and

orientation: (1) the cut samples have a known orientation; (2) from VISAR and computational results, the pressure can be calculated as a function of distance and can be established accurately at the foil plane. The pressure decay is assumed independent of orientation. Therefore, for the [110] monocrystalline Ta sample subjected to a 625 J laser-induced shock pulse, the pressure at a distance 200 μm below the crater (crater depth is about 166 μm) is about 71 GPa. DIFFRACT™ was used to simulate the diffraction patterns taken from TEM images.

3. Results and Discussion

3.1. TEM Diffraction Pattern Simulation

The TEM diffraction patterns for substructures were simulated by the software DIFFRACT. The lattice parameter for bcc Ta is 0.33 nm. For the twin structures in the bcc Ta matrix, the lattice parameters are the same. The crystallographic relations between the twin structure and matrix are listed in Table 1 (the "plane" indicates the twin plane while the "direction" indicates the relation between the twin structure and matrix).

In simulating the diffraction patterns of the Omega phase, the structure identified by Hsiung and Lassila [4–6] was used. It is a pseudo-hexagonal structure and the lattice parameters are listed in Table 2. The locations of the atoms are (0, 0, 0), (0.6853, 0.3146, 0.5), and (0.3146, 0.6853, 0.5), considering that the lattice dimensions are unit. Similar to the twin structure, the relations between Omega phase and bcc matrix are listed in Table 3. In the simulation, the triclinic crystal definition was used.

Using foil normal = [110] and zone axis = [131] as an example, the extra diffraction spots in the diffraction pattern are shown in Fig. 2. It is clear that the twin plane is $(\bar{2}1\bar{1})$, as it is the mirror line between the two pairs of matrix and twin spots, $10\bar{1}$ and $\bar{1}01$, as shown in Fig. 2(a). Fig. 2(b) is the simulated diffraction pattern with the Omega phase substructure spots (hollow circles) in the same matrix and orientation. It is clear that the distribution of extra spots is different from the one for twinning. Therefore, the shock-induced substructure can be identified by the electron diffraction pattern. Similar results for foil normal = [123] and zone axis as [101] are shown in Figs. 2(a). The differences are clear and the Omega phase can be easily identified. The size of the hollow circle represents the intensity.

3.2. BCC to HCP Phase Transformation

The mechanism of phase transformation for bcc to hcp in tantalum was proposed by Hsiung and Lassila [4,5]. The substructures were observed in our experiment after a pulse with a duration of ~3.7 ns, 1/50the of the one used by Hsiung and Lassila [4, 5]. Fig. 3 shows the TEM dark field micrographs for three different orientations: [110] 625 J Ta at ~200 μm below the bottom of the crater; [111] 661 J monocrystalline Ta at 245 μm below the bottom of the crater and [123] 633 J Ta at 200 μm below the bottom of the crater. From the LASNEX simulation results, the corresponding pressure at this position is ~71 GPa. The circles in the inserted diffraction patterns indicate the spots used for dark field images. From the simulation software, DIFFRACT, the matrix diffraction pattern can be identified and indicated that zone <131> for [110], zone <113> for [111] and zone <011> for [123] monocrystalline tantalum.

Comparing the morphology of the phase and the diffraction patterns with the results by Hsiung and Lassila [4, 5], it can be concluded that substructure is the Omega phase. The plate shape of the ω phase suggests that the interface energy plays an important role; there seems to be a process of minimized energy at specific orientations, a common phenomenon in phase boundaries. The Omega domains have a lateral dimension of ~0.2-0.4 μm (Fig. 3(a, b)). These plates are shorter and blockier in [123] monocrystalline Ta (Fig. 3(c)). Hsiung and Lassila [14-16] also observed the formation of zigzag-shape Omega phase that they suggested was due to the coalescence of Omega blocks of the same variant. In this study, the irregular shapes resulting, apparently, from the coalescence of different blocks, are observed as well. The volume fraction of Omega phase in these three orientations also can be calculated from TEM images and is shown in Figure 3. The highest volume fraction occurs for shock compression along the [110] orientation.

EBSD and pole figure experimental results from Florando et al. [15] indicate that twinning in [110] and [123] oriented monocrystals is relatively easier to occur. In this research, the volume fraction of Omega phase is also higher in [110] and [123] orientations as shown in Fig. 4.

Some of the inconsistencies between quasi-static and dynamic observations can be attributed to a deviation from a purely hydrostatic stress in shock compression. The shear (deviatoric) component of stress is significant, and, since the Alpha to Omega transformation requires a shuffle, it is very probable that the shear component of stress contributes to the transformation. Shear stresses have been found to have a significant effect on reactions and

phase transitions. This was first recognized by Bridgman [16] and later, by Teller [17]. Enikopian [18] systematically investigated the effect in polymers and Chen *et al*. [19] showed that the threshold pressure for the exothermic reaction between Ti and Si powders was significantly decreased by the superposition of shear stresses. In shock compression, the shear component is very significant. In tantalum, one has the following ratio between shear stress (τ_{max}) and pressure (p):

$$\frac{\tau_{\max}}{p} = \frac{3(C_{11} - C_{12})}{2C_{12} + C_{11}}$$

where C_{11} =260.9 GPa and C_{12} =165.2 GPa [3] are elastic stiffness for Ta. The ratio is 0.49, using zero pressures values. As plastic deformation and/or shear transformation take place, this value is relaxed.

4. Summary and Conclusions

1. The current results corroborate the discovery of the Omega phase transformation by Hsiung and Lassila [4], observed in explosively accelerated flyer plate impact experiments (t_p ~ 1.8 μs). We report the observation of an Omega (hexagonal) phase in body centered tantalum compressed by shock waves to a pressure of 70 GPa with a attendant temperature of ~1000 K for a duration of 3.7 ns. This is a factor of 500 lower time scale than the previous report by Hsiung and Lassila [4,5]. The nanosecond scale duration in our experiments was accomplished by high energy laser pulses (~650 J) converging on a region with approximately 1 mm diameter on the sample surface.
2. The transformation was observed in recovery specimens from laser-shock experiments for the three orientations [110], [111], and [123].
3. The Omega phase was observed at a peak pressure ~70 GPa. From the current results and Hsiung and Lassila's [4-6] experiments, it can be concluded that the experimentally obtained phase transformation pressure is ~43-68 GPa. This is higher than the twinning threshold stress.
4. The Omega phase has the same blocky structure in the three shock compression orientations. The interface with the matrix is composed of planar regions of preferred orientation. The orientation relationship between the Omega and BCC matrix is:

$$(111)_m // (0001)_\omega$$
$$[1\bar{1}0]_m // [1000]_\omega$$
$$[01\bar{1}]_m // [0100]_\omega$$
$$[10\bar{1}]_m // [1100]_\omega$$
$$[0\bar{1}\bar{1}]_m // [00\bar{1}0]_\omega$$
$$[012]_m // [00\bar{1}2]_\omega$$
$$[311]_m // [00\bar{1}\bar{1}]_\omega$$

5. The threshold pressure for the Omega transformation observed in the current laser shock experiments (~70 GPa) is significantly higher than the one quoted by Hsiung [4,5] (30 GPa for polycrystalline Ta and 45 GPa for Ta-10W alloy). Two possible reasons for the difference are: (a) the much lower pulse duration in laser shock vs. flyer-plate shock. (b) Hsiung and Lassila [4,5] observed the transformation in polycrystalline Ta.

Acknowledgements

This research is funded by the UC Research Laboratories Grant (09-LR-06-118456-MEYM) and the National Laser Users Facility (NLUF) Grant (PE-FG52-09NA-29043). Electron microscopy was conducted at the SHaRE User Facility, which is sponsored at Oak Ridge National Laboratory by the Division of Scientific User Facilities, US Department of Energy. We acknowledge the use of the UCSD Cryo-Electron Microscopy Facility which is supported by NIH grants to Dr. Timothy S. Baker and a gift from the Agouron Institute to UCSD. The help by Dr. B. Kad is gratefully acknowledged.

Prepared by LLNL under Contract DE-AC52-07NA27344

References

[1] L. Burakovsky, S. P. Chen, D. L. Preston, A. B. Belonoshko, A. Rosengren, A. S. Mikhaylushkin, S. I. Simak, and J. A. Moriarty, Phys. Rev. Lett. **104**, 255702 (2010).

[2] J. B. Haskins, J. A. Moriarty, and R. Q. Hood, Phys. Rev. B **86**, 224104 (2012).

[3] S. L. Shang, A. Saengdeejing, Z. G. Mei, D. E. Kim, H. Zhang, S. Ganeshan, Y. Wang, and Z. K. Liu, Comput. Mater. Sci. **48**, 813 (2010).

[4] L. M. Hsiung and D. H. Lassila, Acta Mater. **48**, 4851 (2000).

[5] L. . Hsiung and D. . Lassila, Scr. Mater. **38**, 1371 (1998).

[6] L. L. Hsiung, J. Phys. Condens. Matter **22**, 385702 (2010).

[7] J. Hu, C. Dai, Y. Yu, Z. Liu, Y. Tan, X. Zhou, H. Tan, L. Cai, and Q. Wu, J. Appl. Phys. **111**, 033511 (2012).

[8] D. Errandonea, M. Somayazulu, D. Häusermann, and H. K. Mao, J. Phys. Condens. Matter **15**, 7635 (2003).

[9] M. A. Meyers, F. Gregori, B. K. Kad, M. S. Schneider, D. H. Kalantar, B. A. Remington, G. Ravichandran, T. Boehly, and J. S. Wark, Acta Mater. **51**, 1211 (2003).

[10] B. A. Remington, P. Allen, E. M. Bringa, J. Hawreliak, D. Ho, K. T. Lorenz, H. Lorenzana, J. M. McNaney, M. A. Meyers, S. W. Pollaine, K. Rosolankova, B. Sadik, M. S. Schneider, D. Swift, J. Wark, and B. Yaakobi, Mater. Sci. Technol. **22**, 474 (2006).

[11] M. A. Meyers, F. Gregori, B. K. Kad, M. S. Schneider, D. H. Kalantar, B. A. Remington, G. Ravichandran, T. Boehly, and J. S. Wark, Acta Mater. **51**, 1211 (2003).

[12] H. N. Jarmakani, E. M. Bringa, P. Erhart, B. A. Remington, Y. M. Wang, N. Q. Vo, and M. A. Meyers, Acta Mater. **56**, 5584 (2008).

[13] M. A. Meyers, M. S. Schneider, H. Jarmakani, B. Kad, B. A. Remington, D. H. Kalantar, J. McNaney, B. Cao, and J. Wark, Metall. Mater. Trans. A **39**, 304 (2007).

[14] D. H. Kalantar, J. F. Belak, G. W. Collins, J. D. Colvin, H. M. Davies, J. H. Eggert, T. C. Germann, J. Hawreliak, B. L. Holian, K. Kadau, P. S. Lomdahl, H. E. Lorenzana, M. A. Meyers, K. Rosolankova, M. S. Schneider, J. Sheppard, J. S. Stölken, and J. S. Wark, Phys. Rev. Lett. **95**, (2005).

[15] J. N. Florando, N. R. Barton, B. S. El-Dasher, J. M. McNaney, and M. Kumar, J. Appl. Phys. **113**, 083522 (2013).

[16] P. Bridgman, Phys. Rev. **48**, 825 (1935).

[17] E. Teller, J. Chem. Phys. **36**, 901 (1962).

[18] N. S. Enikolopian, Pure Appl. Chem. **57**, 1707 (1985).

[19] H. C. Chen, J. C. Lasalvia, V. F. Nesterenko, and M. A. Meyers, Acta Mater. **46**, 3033 (1998).

Tables:

Table 1: Parameter relations for twin structure used in DIFFRACT software.

Plane	Direction
$(21\bar{1})_m // (21\bar{1})_t$	$[1\bar{1}1]_m // [\bar{1}1\bar{1}]_t$
$(2\bar{1}1)_m // (2\bar{1}1)_t$	$[11\bar{1}]_m // [\bar{1}\bar{1}1]_t$
$(2\bar{1}\bar{1})_m // (2\bar{1}\bar{1})_t$	$[111]_m // [\bar{1}\bar{1}\bar{1}]_t$
$(211)_m // (211)_t$	$[\bar{1}11]_m // [1\bar{1}\bar{1}]_t$
$(1\bar{1}2)_m // (1\bar{1}2)_t$	$[\bar{1}11]_m // [1\bar{1}\bar{1}]_t$
$(\bar{1}\bar{1}2)_m // (\bar{1}\bar{1}2)_t$	$[111]_m // [\bar{1}\bar{1}\bar{1}]_t$
$(\bar{1}12)_m // (\bar{1}12)_t$	$[1\bar{1}1]_m // [\bar{1}1\bar{1}]_t$
$(112)_m // (112)_t$	$[11\bar{1}]_m // [\bar{1}\bar{1}1]_t$
$(121)_m // (121)_t$	$[1\bar{1}1]_m // [\bar{1}1\bar{1}]_t$
$(\bar{1}21)_m // (\bar{1}21)_t$	$[11\bar{1}]_m // [\bar{1}\bar{1}1]_t$
$(\bar{1}2\bar{1})_m // (\bar{1}2\bar{1})_t$	$[111]_m // [\bar{1}\bar{1}\bar{1}]_t$
$(12\bar{1})_m // (12\bar{1})_t$	$[\bar{1}11]_m // [1\bar{1}\bar{1}]_t$

Table 2: Parameters for pseudo hexagonal structure of Omega phase in Ta.

a	b	c	α	β	γ
0.467 nm	0.467 nm	2.86 nm	90°	90°	120°

Table 3: Parameters relation for Omega phase used in DIFFRACT software.

Plane	Direction
$(111)_m // (001)_\omega$	$[1\bar{1}0]_m // [100]_\omega$
$(111)_m // (001)_\omega$	$[01\bar{1}]_m // [010]_\omega$
$(111)_m // (001)_\omega$	$[10\bar{1}]_m // [110]_\omega$
$(0\bar{1}1)_m // (\bar{1}1\bar{1})_\omega$	$[0\bar{1}\bar{1}]_m // [\bar{1}\bar{1}0]_\omega$
$(200)_m // (02\bar{1})_\omega$	$[012]_m // [\bar{1}\bar{1}2]_\omega$
$(0\bar{1}1)_m // (01\bar{1})_\omega$	$[311]_m // [\bar{1}\bar{1}\bar{1}]_\omega$

Figures:

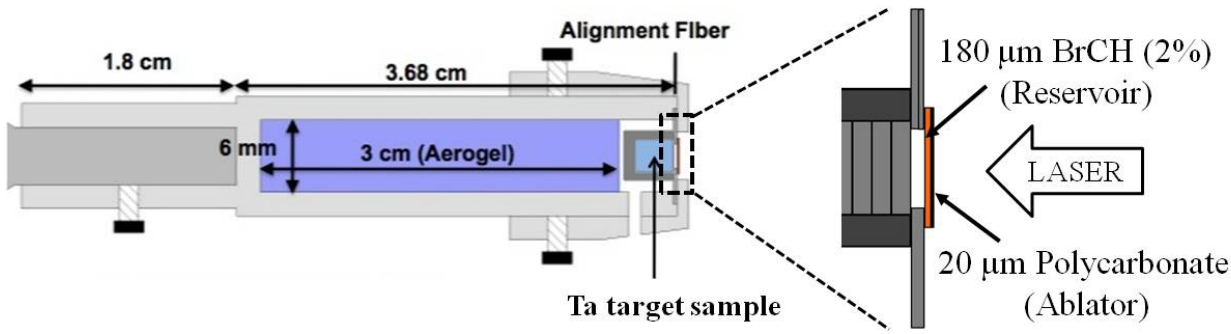

(a)

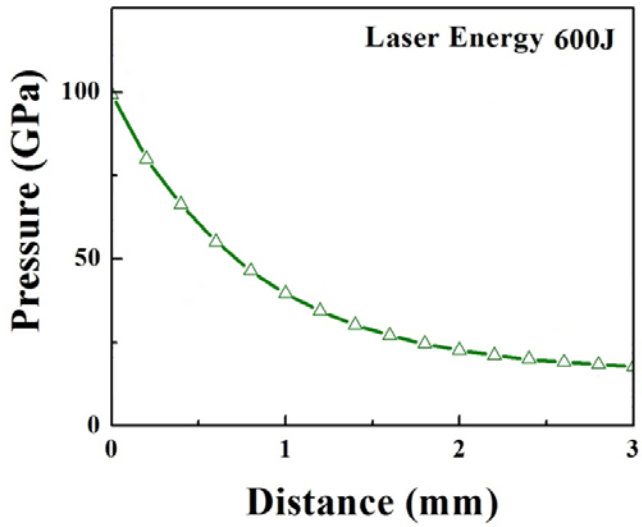

(b)

Figure 1: (a) Assembly used to shock compress the Ta monocrystals; notice momentum trap; (b) calculated pressure (using 1-D LASNEX and normalization parameter) as a function of depth for laser shock energy of 600 J.

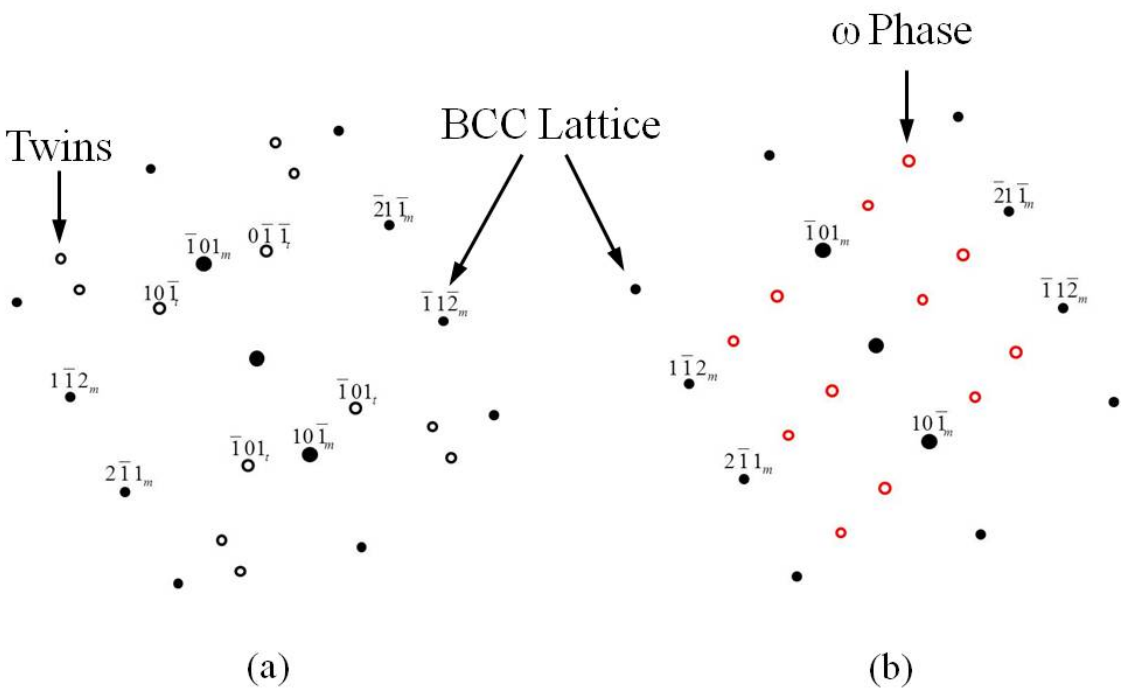

Figure 2: Simulated diffraction pattern with (a) twin spots (hollow circles and subscript t) and (b) Omega phase spots (hollow circles). Foil normal [110] and zone axis [131].

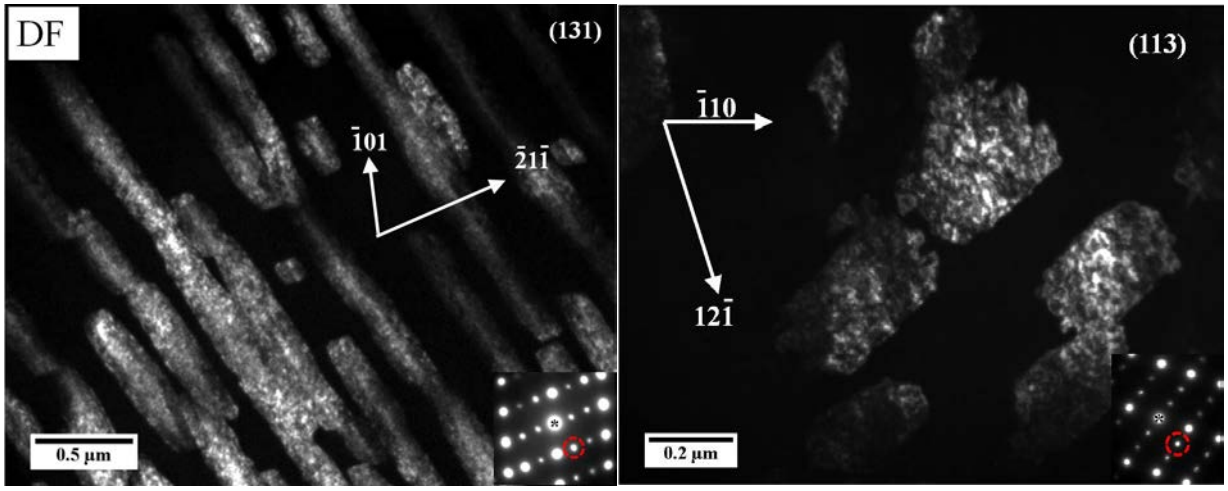

(a) (b)

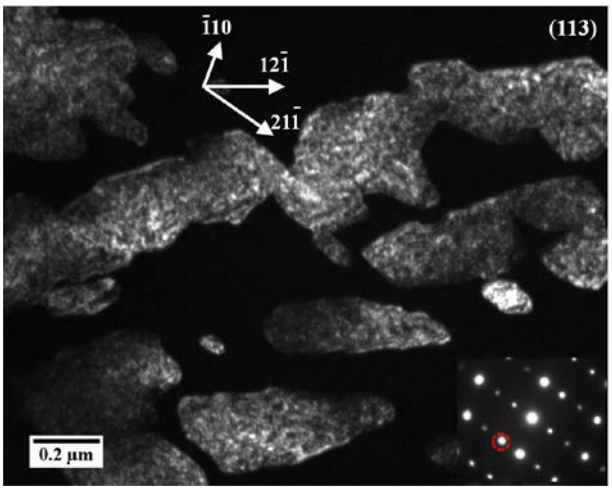

(c)

Figure 3: Dark-field TEM images showing ω phase (bright areas) in (a) [110] monocrystalline Ta driven energy of 625 J (foil at 200 µm below the crater, corresponding to pressure of ~ 71 GPa); (b) [111] monocrystalline Ta driven energy of 661 J (foil at 245 µm below the crater, corresponding to pressure of ~ 71 GPa); (c) [123] monocrystalline Ta driven energy of 633 J (foil at 200 µm below the crater, corresponding to pressure of ~ 72 GPa). The enlightened spots are circled in inserted diffraction patterns.

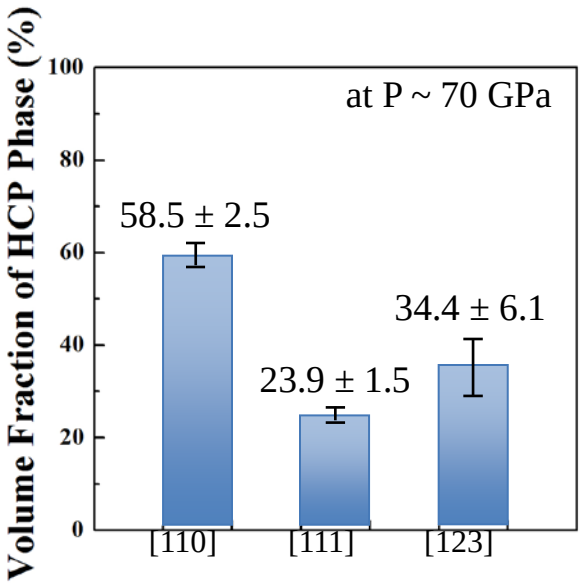

Figure 4: Volume fraction of HCP phase in [110], [111] and [123] monocrystal orientation at energy of ~70 GPa. The [110] has the highest Omega phase density.